U. S. Department of the Interior
Geological Survey

INTERPRETATION OF TIME-DOMAIN ELECTROMAGNETIC SOUNDINGS IN THE EAST RIFT GEOTHERMAL AREA OF KILAUEA VOLCANO, HAWAII

by

Jim Kauahikaua

Open-File Report 81-979

1981

INTERPRETATION OF TIME-DOMAIN ELECTROMAGNETIC SOUNDINGS IN THE EAST RIFT GEOTHERMAL AREA OF KILAUEA VOLCANO, HAWAII

by Jim Kauahikaua

INTRODUCTION

A controlled-source time-domain electromagnetic (TDEM) sounding survey was completed on the lower portion of the East Rift of Kilauea Volcano, Hawaii (locally known as the Puna area) during the summer of 1974 as part of the geophysical task of the Hawaii Geothermal Project. The data have been interpreted previously using a simple half-space model (Klein and Kauahikaua, 1975; Kauahikaua and Klein, 1977b and 1978); however, this report presents interpretations as obtained by a layered-earth TDEM inversion computer program. The interpretations in terms of uniform half-space models were adequate for delineating the lateral extent of low-resistivity areas, but interpretations in terms of layered half-space models can be used to localize low-resistivity zones vertically as well as horizontally. The results show that much of the area is underlain by an anomalously conductive zone at depths of 250 to 1,300 below sea level.

Twenty-four TDEM soundings were attempted in the area using four different grounded wire current sources and a 42-conductor, horizontal loop sensor. The TDEM sounding data were in the form of voltages (proportional to the time derivative of the induced magnetic field) measured at discrete times after a break in the source current. Seventeen of the soundings are interpreted here (locations shown in fig. 1). Details of data acquisition and reduction are given by Kauahikaua and Klein (1977b).

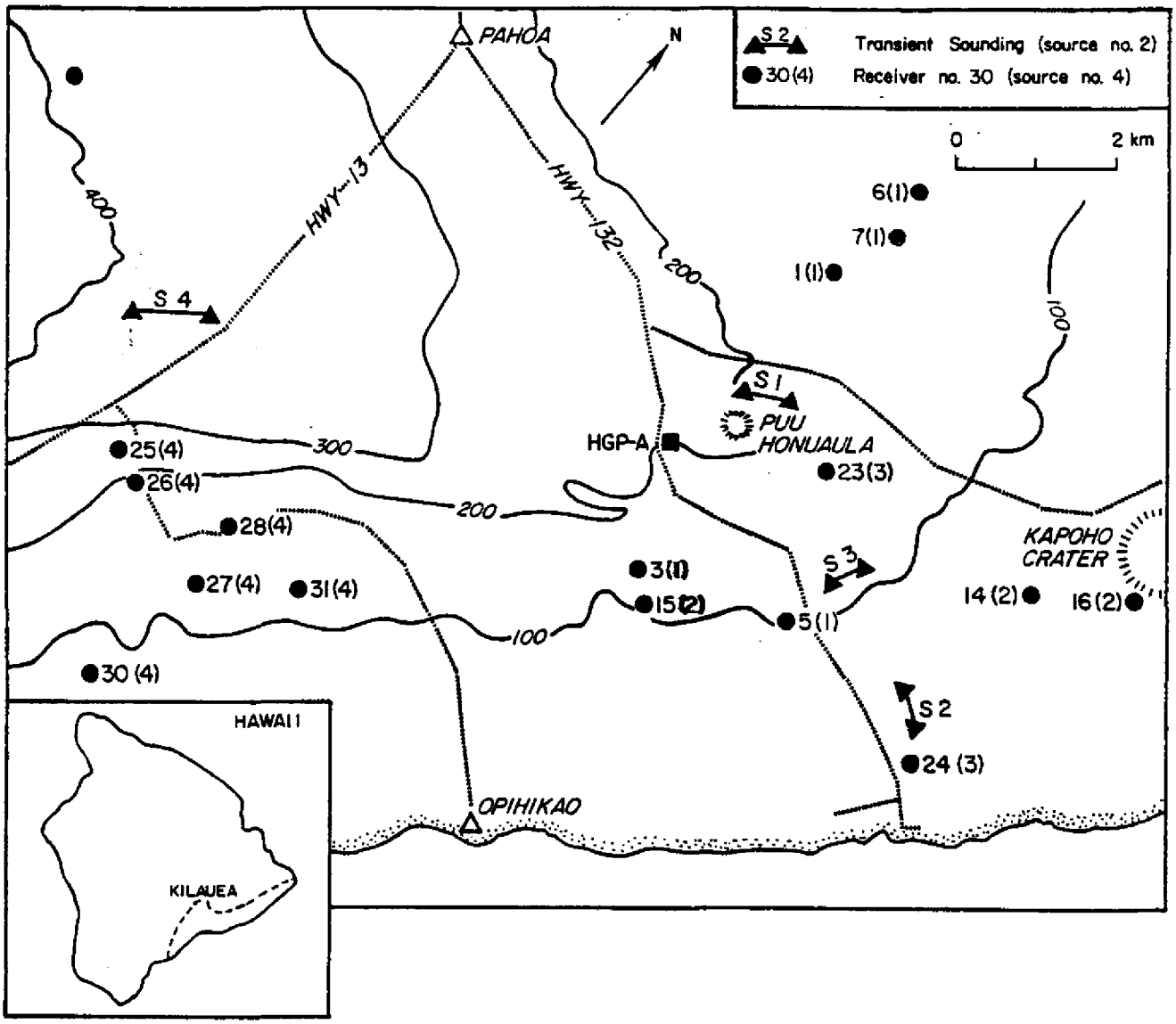

Figure 1. Map of the lower East Rift zone of Kilauea volcano, Hawaii, showing prominent roads and topographic features. Also shown are the locations of the grounded-wire sources and horizontal-loop receivers used in the soundings interpreted in this report.

INTERPRETATIONAL PROCEDURE

Interpretation of the reduced vertical field TDEM data was done by automatically minimizing the squared differences between data and theoretical TDEM responses to layered earth models using program MQLVTHXYZ (Kauahikaua, 1980). For an m-layered model, this computer program determines 2*m parameters: m-layer conductivities, (m-1) thicknesses, and an amplitude scaling factor. For each sounding, the best fitting layered model parameters and parameter errors, a parameter correlation matrix, and a data and model-response plot are included in the appendix. Layer conductivities will also be discussed as resisitivities; to convert from one to the other, resistivity is the reciprocal of conductivity. The parameter errors are listed as percentages of the parameter value. The correlation coefficients, which describe the relative amount of variance in the data explained by a linear relationship between two parameters are listed as dimensionless numbers between either -1.0 and + 1.0, or -100 percent and +100 percent.

Use of the layered-earth models for each of the soundings is only valid when the actual electric structure changes very slowly in any lateral direction. The extent to which lateral variation in structure will invalidate the layered model approach is not known; however, self-consistency in earth models derived from a variety of source-sensor combinations in an area would be a strong indication that the layered-model approach is pretty good. The purpose of including an amplitude-scaling factor in the layered model is to further minimize the effects of lateral variations by simplistically accounting for anomalous current buildup at lateral boundaries; it is assumed that the relative decay behavior of the magnetic field would still be a function of the conductivities present at depth.

RESULTS OF THE LAYERED HALF-SPACE INVERSION

For each inversion, the number of layers in the model was increased until there was no apparent improvement in the match of the data to the model responses (until the standard error of fit no longer decreased). The purpose of this strategy was to obtain, by inversion, the simplest layered-earth model that would describe the significant features of the data. The standard error of fit should be approximately equal to the average error in the data in this case. All but soundings 6, 15, and 23 had standard errors of fit that were comparable to the average error in the data (about 5 percent of the largest data value).

Most of the sounding data were adequately fit by three-layer model responses whose layer conductivities increased with depth. The only exceptions were three soundings (numbers 14, 15, and 16) from the same source, which required three-layer models with a thin, surface layer that was more conductive than the second layer. The similarity of first-layer properties in the three soundings at different places but using the same source, along with the dissimilarity of first-layer properties in two soundings at the same place but using different sources (numbers 5 and 15), strongly suggests that the conductive first layer is more representative of the shallow structure beneath source 2; however, the deeper structure is more representative of the receiver location, as evidenced by the similarity of second-layer parameters for the two soundings at the same location using different sources (5 and 15).

Four soundings required less than three layers in their best fit models. Soundings 25 and 26 were very difficult to fit with a layered-earth response; this, coupled with their extreme closeness to the source, suggests that the

two sets of sounding data may be distorted by some shallow structure in the immediate vicinity of the source. Because of our inability to quantify or correct such distortions, these two soundings will not be included in the geologic interpretation, although their interpretations are listed in the appendix. Soundings 24 and 29 are fit well by the layered-earth models and are identical to the bulk of the soundings except for the absence of the first layer in the general three-layer model. That is to say that the first layer in soundings 24 and 29 is very similar to the second layer found in the bulk of the three-layer earth interpretations. The first layer is poorly resolved when it is included in a three-layer interpretation; therefore it shouldn't be surprising that the first layer (of a three-layer earth) may not be resolved at all in a few of the data sets. It will be assumed that the first layer of soundings 24 and 29 is comparable to the second layer of any of the three-layer models.

Of all the earth-model parameters, the properties of the first layer (layer 1) were resolved to the poorest degree. The estimated parameter errors were much larger for these parameters, and the absolute value of their correlation coefficients was generally above the 89 percent level. The reason for the poor resolution and high parameter correlation was a combination of the known high resistivities of rocks above sea level and the lack of data at times small enough to resolve such resisitivites. Schlumberger DC soundings in Puna have measured a representative resistivity of 6,000 ohm-m for the undersaturated rock above the water table (Kauahikaua and Klein, 1977a). A TDEM sounding would require data at times of about three orders of magnitude smaller than the earliest time of 20 msec used in this study to resolve such a resistivity. The interpreted first-

layer conductivities are probably no more than upper limits and are therefore of no real value. The following discussion will concentrate on the deeper parameters and will disregard the layer-1 parameters determined by inversion, except to assume that layer-1 represents the undersaturated rocks above sea level.

The parameters of layer-2 are resolved to a significantly better degree than those of the surface layer. Resistivities range from 1.9 to 6.3 ohm-m (with the exception of the value of 40 ohm-m for sounding 29), in excellent agreement with previously determined values (Kauahikaua and Klein, 1977a; Keller and others, 1977). Thicknesses range from 250 m to 1,300 m. The top of layer-2 is fixed near sea level by the above assumptions for layer-1, and so these thicknesses can also be thought of as depths below sea level to basement. Layer-2 resisitivities and thicknesses are contoured in figures 2 and 3, respectively.

The estimated errors in both the resistivity and thickness of layer-2 are roughly 80 percent for most soundings, even though the two are strongly correlated (correlation coefficient between conductivity and thickness of -95 percent and -100 percent). The large magnitude of the errors is due mainly to the correlation, since each parameter error estimate is computed assuming complete parameter independence. This linear dependence implies that the layer-2 conductance (thickness times conductivity) is better determined than either parameter alone, but that there is a relatively limited range of values for which each parameter satisfies the conductance relation and fits the data. An excellent discussion on the accuracy of parameter estimation through inversion can be found in Inman (1975).

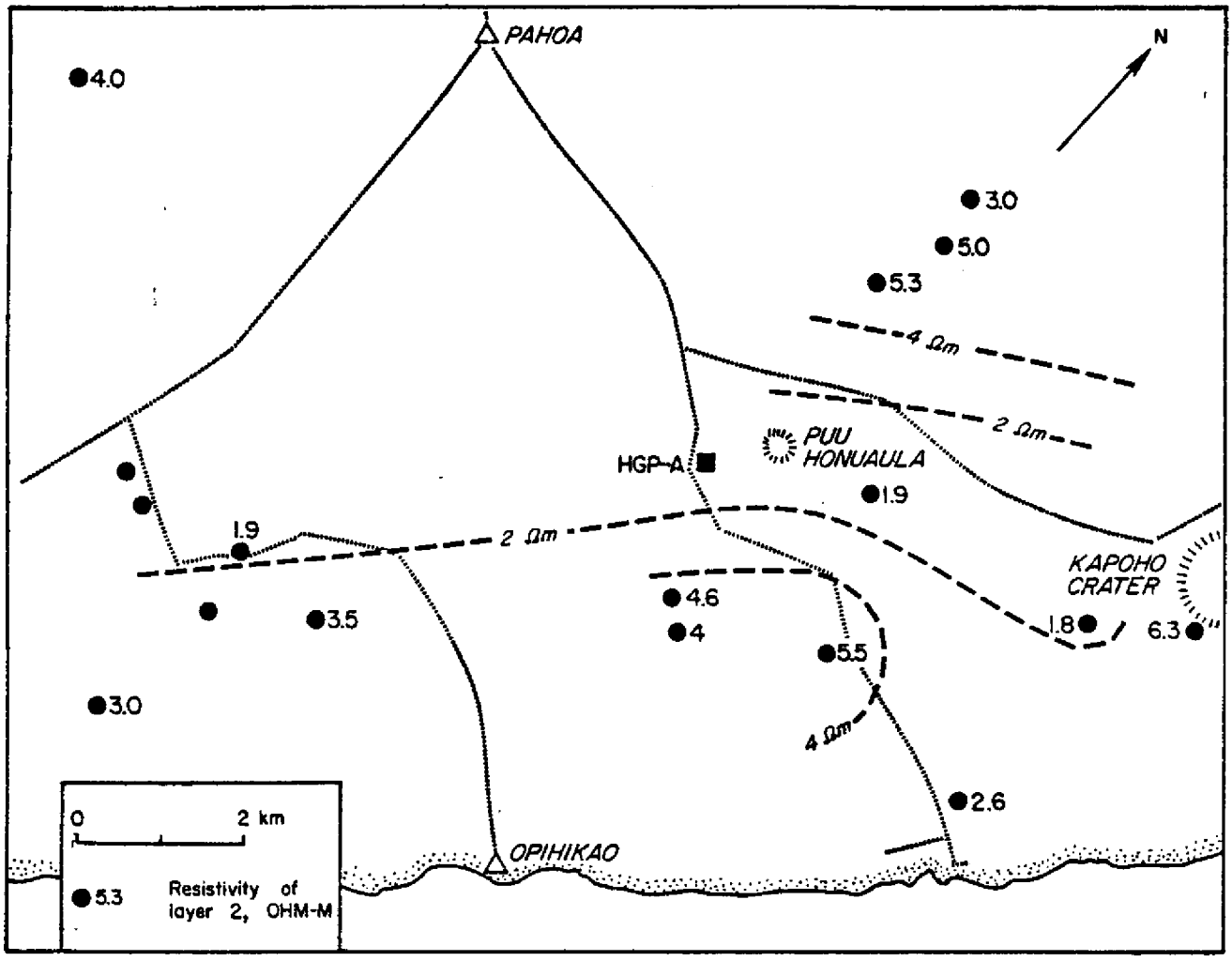

Figure 2. Contoured values of second-layer resistivity, in ohm-m.

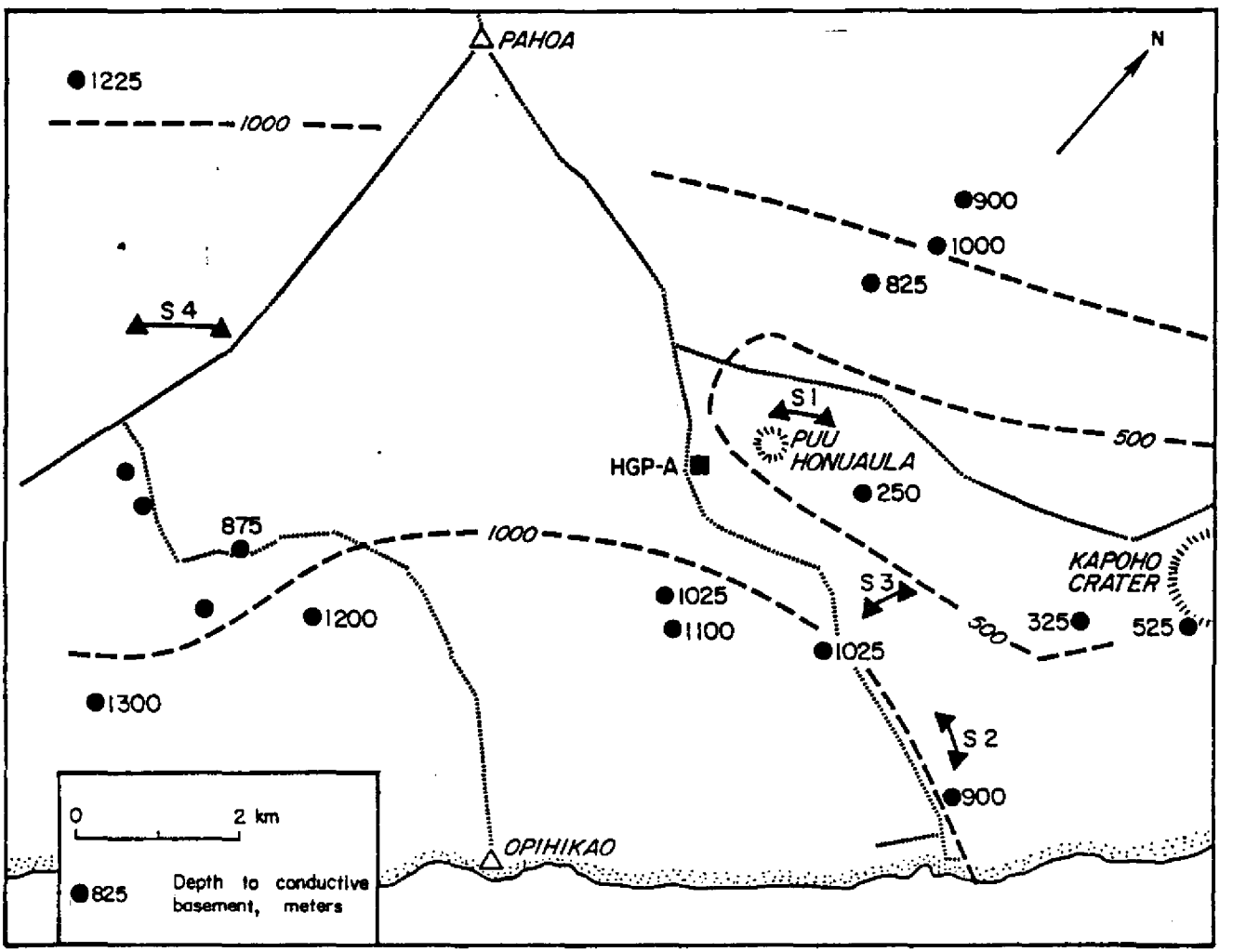

Figure 3. Contoured values of second-layer thickness, or depth below sea level to conductive basement, in meters.

The sole exception is sounding 27. Layer-2 conductivity and thickness are perfectly correlated (correlation coefficient of -1.0) in this sounding's interpretation. These parameters appear to be made either extremely big or extremely small by the strong correlation compared to the three soundings around it, even though its conductivity-thickness product is similar to that for sounding 28. This suggests that the actual values of layer-2 conductivity and thickness are not sufficiently resolved to be used separately. The values for sounding 27 have been excluded from figures 2 and 3.

Examination of the contoured maps for layer-2 properties shows that the rift zone has a different electrical structure than the areas to either side. Resistivities become lower and the layer thicknesses become thinner as the rift is approached. In light of the strong correlation between these two parameters, the layer-2 conductances were scrutinized to ascertain whether the resistivity and thickness variations were independent in magnitude, or whether they were linearly dependent to the extent that a constant conductance was being estimated for all Puna soundings. The layer-conductance estimates varied a great deal, but were generally smaller within the rift zone; the estimates range from 87 mhos for sounding 16 in the rift zone to 430 mhos for sounding 30 south of the rift zone. The parameter variations seem to indicate a genuine thinning of layer-2 within the rift zone accompanied by a decrease in resistivity.

The westernmost sounding (number 29) is very different from the rest of the Puna soundings. The range of resistivities characteristic of layer-2 in the other 16 soundings is only encountered in sounding 29 at depths greater than 1,200 m. Earlier bipole-mapping and TDEM survey results from the area near sounding 29 show the subsurface to have a resistivity of 15 to

20 ohm-m (Keller and others, 1977); the estimate from sounding 29 is 40 ohm-m to a 1,200 m depth, and 5 ohm-m below that level. These data suggest that the electrical structure north of the rift and west of Pahoa is significantly more resistive than the rest of Puna.

The electrical properties of the basement (layer-3) were very poorly determined, although the inversion runs invariably required a third layer to obtain an adequate fit to the data. Eleven of the 14 three-layer models had conductive basements with resistivities ranging from 2.3 ohm-m to 0.05 ohm-m. The layer-3 resistivity error estimates were very high and the resistivities did not exhibit any spatial trends. The total impression one gains from this analysis is that the TDEM sounding data did not have sufficient resolution to obtain reliable estimates of the deep conductivities for every sounding; however, on the average, layer-3 appeared to be more conductive than layer-2. A previous TDEM survey covering the area to the west of HGP-A also detected a conductive basement at depths generally exceeding 900 m below sea level in many of their soundings southeast of the rift and within the rift near HGP-A (Skokan, 1974), substantiating the findings presented here.

GEOLOGICAL IMPLICATIONS OF THE DATA

The increase in bulk conductivity at depths on the order of 1 km cannot be due solely to increases in porosity. (Moore, 1965, demonstrates that porosity generally decreases with depth beneath Hawaii.) Neither can it be due solely to increases in salinity (pore fluids grade quickly into seawater with depth below sea level beneath most of this area). The bulk-conductivity increase must be due primarily to the effects of heat at depth. Conductivities do increase with depth in the logs of well HGP-A (Rudman, 1978), substantiating

this hypothesis. Utilizing the test well HGP-A as a control point and assuming that the high conductivities at depth are caused principally by the effects of heat, the basement surface could represent an isotherm of approximately 200 to 250 degrees C.

Studies of groundwater temperatures in shallow wells (less than 50 m below sea level) in the East Rift area show that temperatures at the water-table surface can exceed 90 degrees C locally within the rift structure and 40 degrees C on the flanks near the rift, but that the temperatures decrease rapidly with depth (Epp and Halunen, 1979). The bulk of the shallow groundwater must be at temperatures less than 30 to 40 degrees C with shallow-rift-zone heat sources being responsible for the thin, high-temperature fluid layer at the surface. Hypothesizing a widespread temperature increase to 250 degrees C at depths between 1,000 and 1,300 m below sea level beneath an area as large as the East Rift (including the area beneath the flanks of the rift structure) while shallow groundwater temperatures remain relatively low requires some sort of barrier to vertical fluid flow. Some barrier must also be hypothesized to explain the increase in temperature gradients in HGP-A from a normal 30 degrees C/km in the first 750 m to approximately 570 degrees C/km between 1,000 and 1,200 m.

Zones that could form a barrier have already been discovered through studies of the cores and rock cuttings obtained during the drilling of HGP-A. Stone and Fan (1978) concluded that "all vesicles and fractures [in the cores] appear to be completely filled . . ." with secondary minerals between 1,350 and 1,894 m, thereby reducing actual porosity. On the basis of examinations of the rock cuttings, Palmiter (1976) also described filling of fractures and vesicles by secondary minerals between 670 and 1,050 m; however, the

mineralization was reported as absent between 1,050 and 1,370 m. Palmiter was careful to point out that the decrease in rock porosity does not necessarily mean that bulk fluid permeability has also decreased; in fact, he rated the permeability of the 520 to 1,370 m interval as high, insofar as this reflects inter-flow open spaces and glass fracturing.

These zones of completely filled vesicles would certainly inhibit vertical movement of fluids through individual lava flows, but not necessarily the lateral flow of fluids between successive flows. Bulk permeability of Hawaiian lavas is normally anisotropic, with the highest permeability parallel to the lava's flow direction and the lowest permeability in the vertical direction (Takasaki and Valenciano, 1969, p. 7-10). Filling of vesicles would only accentuate the anisotropy by reducing vertical, not lateral, permeability.

The situation is very different within the rift zone. Intense fracturing and faulting parallel to the rift trend, as well as dike intrusion along zones of weakness within the rift, would decrease fluid permeability normal to the rift and probably enhance the vertical permeability along the fractures. Heated fluids from depth could rise vertically to shallow depths within the rift, but would be confined to flowing laterally away from the rift at depth. A map of prominent eruptive and structural features of the East Rift area (shown as fig. 4) shows areas where shallow, high-temperature waters might be expected to have risen higher than beneath the flanks. Note that the zone of shallow basement in fig. 3 is within mapped rift fissures downrift of HGP-A.

The thermal structure changes drastically when moving north from the rift in the area west of Pahoa. Based on one sounding, the saturated rocks have a resistivity of about 40 ohm-m, which is typical for cold, seawater-

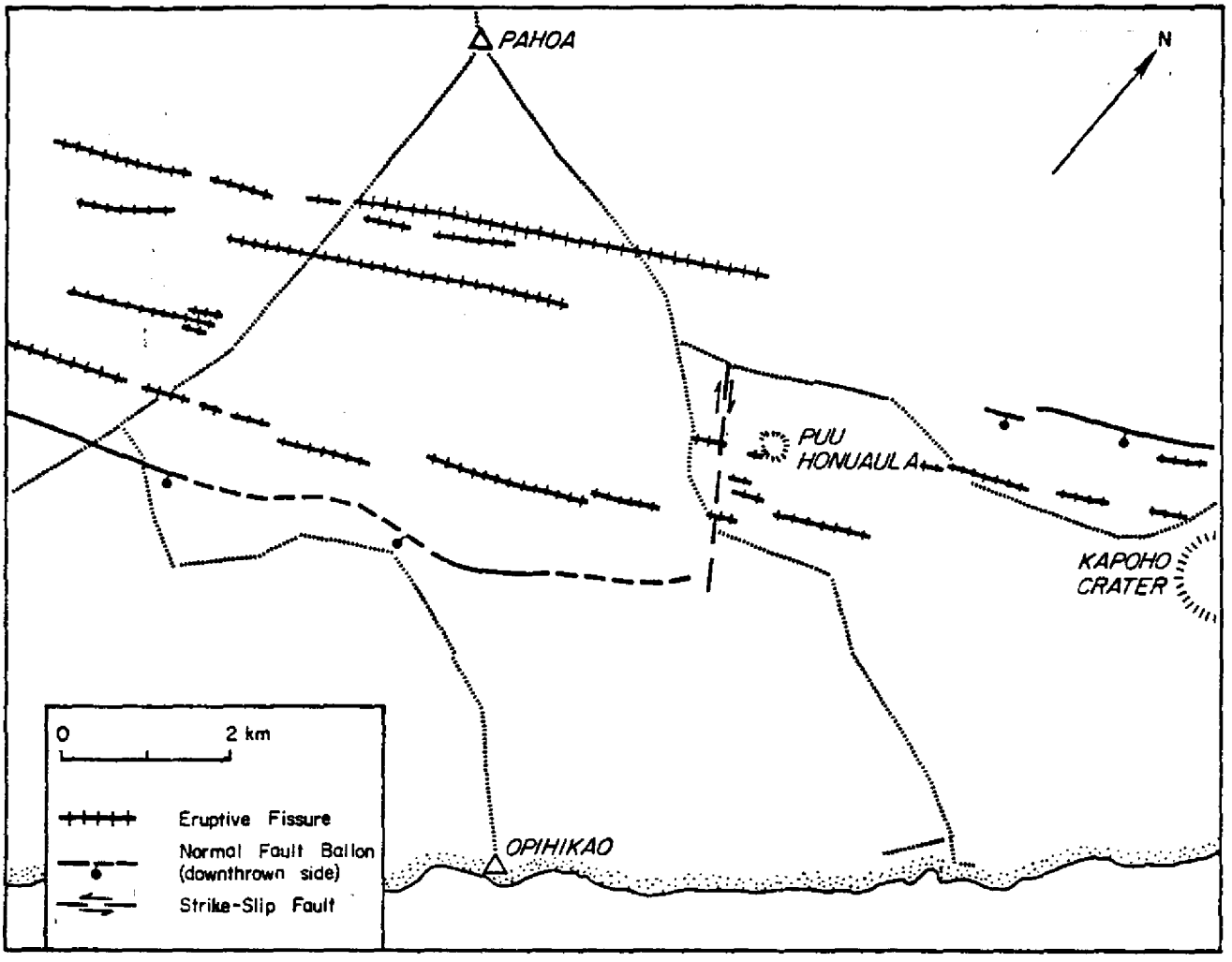

Figure 4. Sketch map of prominent structures of the east rift, after Holcomb (1980).

saturated basalt (Zohdy and Jackson, 1969). Below 1,200 m, this resistivity decreases to about 5 ohm-m. Using the same arguments about resistivity changes with depth as before, the decrease in resistivity must be due to a temperature increase. Areas near the rift which had groundwater temperatures of 30-50 degrees C also had saturated rock resistivities of 5-6 ohm-m. Taking into account the probable decrease in porosity at such depths, the estimated temperature at 1,200 m in the area north of the rift and west of Pahoa must be greater than 30-50 degrees C but probably less than 90 degrees C.

The differences in thermal structures of the two areas reflect differences in their hydrologic characteristics. Northwest of the rift lies possibly the greatest supply of fresh basal-water on the island of Hawaii. The hydraulic gradients are high, and the groundwater discharges directly into the ocean at a rate estimated to be several hundred million gallons per day (Davis and Yamanaga, 1973, p. 34). On the southeastern side of the rift, groundwater is brackish and hydraulic gradients are low; this is due mostly to the rift structure acting as a barrier to southward movement of groundwater from the high recharge areas north of the rift (Davis and Yamanaga, 1973). The high flux of cold water through the rocks north of the rift can act as a very effective heat sink and probably keeps the groundwater uniformly cool to the depth below which lateral fluid flow becomes significantly diminished. No such heat sink exists within the rift or southeast of it; therefore thermal effects are seen more clearly and at shallower depths.

CONCLUDING REMARKS

A zone of high-temperature fluids is proposed to exist at depths greater than 1 km beneath most of the East Rift geothermal area south of the rift and east of Pahoa. Filling of vesicles within horizontal zones at

depths greater than 600 m probably prevents the vertical mixing of these deep fluids with the cooler groundwater at shallow depths, except where the zones are broken up by vertical faulting and fracturing (within the rift itself). The high-temperature fluids appear to be only a few hundred meters below sea level within the eastern portion of the rift zone.

There are two important consequences of this model for geothermal development in Puna. First, if high-temperature fluids do exist beneath such a large area, estimates of the total power content published previously may be too low. A realistic estimate of the total heat in Puna must include the volume of this stratum of hot water, as well as the volume of the rift structure itself. Second, the portion of the rift northeast of HGP-A appears to be as promising as, if not more promising a prospect than, the rift to the southwest. Skokan's (1974) very detailed coverage of the upper portion of the rift did detect the layer-3 described here, but did not find it at the anomalously shallow depths that were found, by this study, in the lower portion of the rift. Drilling in this lower portion of the rift may yield temperatures comparable to those found in HGP-A, but at depths as much as 800 m shallower.

REFERENCES

Davis, D. A., and Yamanaga, G., 1973, Water resources summary: island of Hawaii: Hawaii Div. Water and Land Devel. Report R47, 42 p.

Epp, D., and Halunen, A. J. Jr., 1979, Temperature profiles in wells on the island of Hawaii: Hawaii Inst. of Geophysics Technical Report HIG-79-7, 31 p.

Holcomb, R. T., 1980, Preliminary geologic map of Kilauea volcano, Hawaii: U. S. Geological Survey Open-File Report 80-796, 2 sheets.

Inman, J. R., 1975, Resistivity inversion with ridge regression: Geophysics, v. 40, p. 798-817.

Kauahikaua, J., 1980, Program MQLVTHXYZ: Computer inversion of three-component, time-domain, magnetic-field sounding data generated using an electric wire source: U. S. Geologic Survey Open-File Report 80-1159, 109 p.

Kauahikaua, J. and Klein, D. P., 1977a, Electromagnetic induction sounding measurements in the Puna district, in Geoelectric Studies on the East Rift, Kilauea Volcano, Hawaii Island: Hawaii Inst. of Geophysics Technical Report HIG-77-15, p. 91-119.

----------, 1977b, Interpretation of electromagnetic transient soundings made on the east rift of Kilauea volcano, Hawaii, in Geoelectric Studies on the East Rift, Kilauea Volcano, Hawaii Island: Hawaii Inst. of Geophysics Technical Report HIG-77-15, p. 121-173.

----------, 1978, Results of electric surveys in the area of Hawaii Geothermal Test Well HGP-A: Geothermal Resources Council Transactions, v. 2, p. 363-366.

Keller, G. V., Skokan, C. K., Skokan, J. J., and Daniels, J., 1977, Electrical resistivity and time-domain electromagnetic surveys of the Puna and Ka'u districts, Hawaii county, Hawaii, in Geoelectric Studies on the East Rift, Kilauea Volcano, Hawaii Island: Hawaii Inst. of Geophysics Technical Report HIG-77-15, p. 1-89.

Klein, D. P., and Kauahikaua, J., 1975, Geoelectric-geothermal exploration on Hawaii Island: Preliminary results: Hawaii Inst. of Geophysics Technical Report HIG-75-6, 23 p.

Moore, J. G., 1965, Petrology of deep-sea basalt near Hawaii: Am. J. Sci., v. 263, p. 40-52.

Palmiter, D. B., 1976, Geology of HGP-A from macroscopic study of cores and cuttings: unpublished manuscript, Hawaii Inst. of Geophysics, 8 p.

Rudman, A. J., 1978, Analysis of geophysical logs from the Hawaii Geothermal Project Well: Hawaii Inst. of Geophysics Technical Report HIG-78-9, 25 p.

Skokan, C. K., 1974, A time-domain electromagnetic survey of the East Rift zone, Kilauea volcano, Hawaii: Colorado School of Mines, Ph.D. thesis no. 1700, 150 p.

Stone, C., and Fan, P.F., 1978, Hydrothermal alteration of basalts from Hawaii Geothermal Project Well-A, Kilauea, Hawaii: Geology, v. 6, p. 401-404.

Takasaki, K. J., and Valenciano, S., 1969, Water in the Kahuku area, Oahu, Hawaii: U. S. Geological Survey Water-Supply Paper 1874, 59 p.

Zohdy, A. D. R. and Jackson, D. B., 1969, Application of deep electrical soundings for groundwater exploration in Hawaii: Geophysics, v. 34, p. 584-600.

APPENDIX

For each sounding, this appendix contains a log-log plot of the data and best-fitting model responses, a listing of the best-fit model parameters and their estimated errors, and the parameter correlation coefficient matrix. The best-fit model parameters are layer conductivities in mho/m (denoted by a lower case Greek sigma), layer thicknesses in m (denoted by a lower case 'd'), and an amplitude scaling factor (denoted fctr). Subscripts on the layer conductivity and thickness symbols denote the layer being specified.

The parameter errors are estimated using the derivatives of the best-fit model with respect to each of the parameters. They are listed in this appendix as percentages of the best-fit parameter value. This assumes that the best-fit parameter estimates are linear-normally distributed. Actually, these parameters are log-normally distributed; however, parameter error estimates for linear- or log-normal distributions become almost identical for small errors. For large errors, the estimates are very poor regardless of the type of distribution. Therefore, the parameter error estimates require some interpretation. Experience has shown that the error estimates, as computed in MQLVTHXYZ, are quantitatively accurate when they are less than 50 percent of the parameter value. Above 50 percent the errors can only be used as qualitative measures of the poorness of resolution. The word 'big' is used in place of an error estimate in this appendix when the error is greater than 200 percent of the parameter. The word 'fixed' is used in place of an error estimate when the parameter was so poorly resolved that it needed to be held constant during inversion.

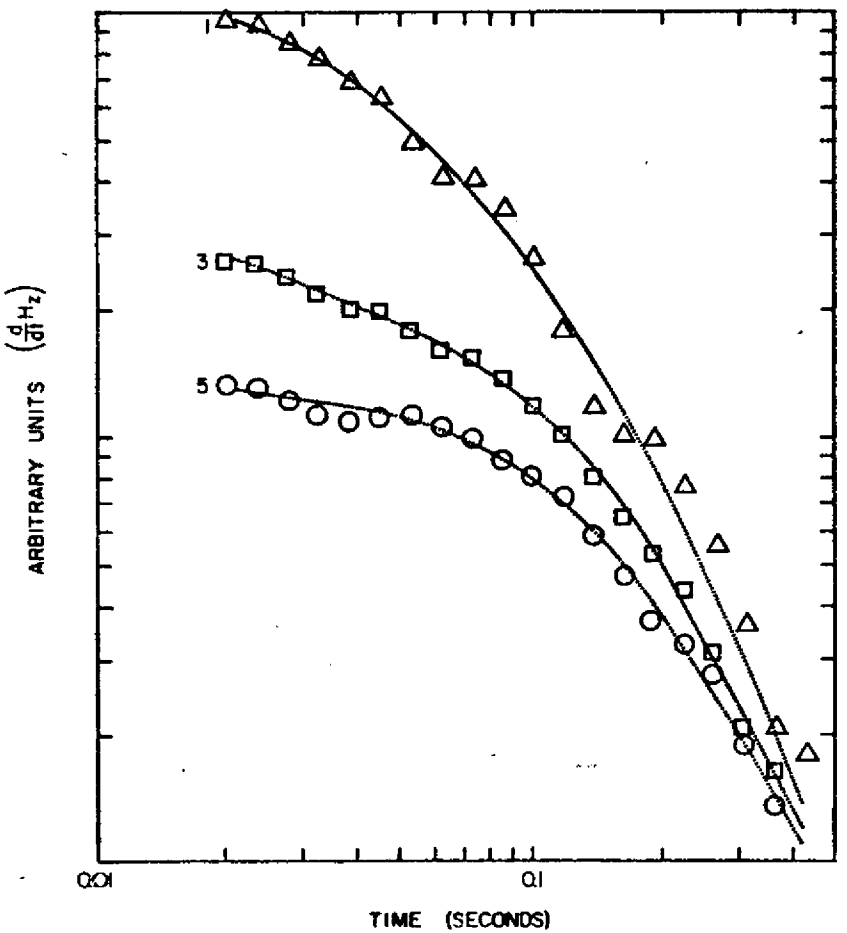

Puna TDEM sounding 1(1)
parameter correlation matrix

	σ_1	σ_2	σ_3	d_1	d_2
σ_2	.78				
σ_3	.59	.90			
d_1	.99	.79	.60		
d_2	-.79	-.90	-.92	-.82	
fctr	-.25	.39	.51	-.26	-.16

final parameters

σ_1	.127	± 38%
σ_2	.190	± 31%
σ_3	.015	± big
d_1	294.	± 90%
d_2	825.	±121%
fctr	1.078	± 9%

Puna TDEM sounding 3(1)
parameter correlation matrix

	σ_1	σ_2	σ_3	$_1$	$_2$
σ_2	.98				
σ_3	.40	.43			
d_1	.90	.81	.38		
d_2	-.95	-.98	-.28	-.75	
fctr	.94	.99	.40	.71	-.98

final parameters

σ_1	.097	± 35%
σ_2	.22	± 49%
σ_3	2.5	± 96%
d_1	383.	± 19%
d_2	1029.	± 67%
fctr	1.355	± 20%

Puna TDEM sounding 5(1)
parameter correlation matrix

	σ_1	σ_2	σ_3	d_1	d_2
σ_2	.86				
σ_3	.53	.85			
d_1	.97	.71	.34		
d_2	-.88	-.95	-.68	-.75	
fctr	.58	.91	.91	.36	-.84

final parameters

σ_1	.118	± 73%
σ_2	.183	± 43%
σ_3	.60	±157%
d_1	280.	±144%
d_2	1016.	± 84%
fctr	1.809	± 22%

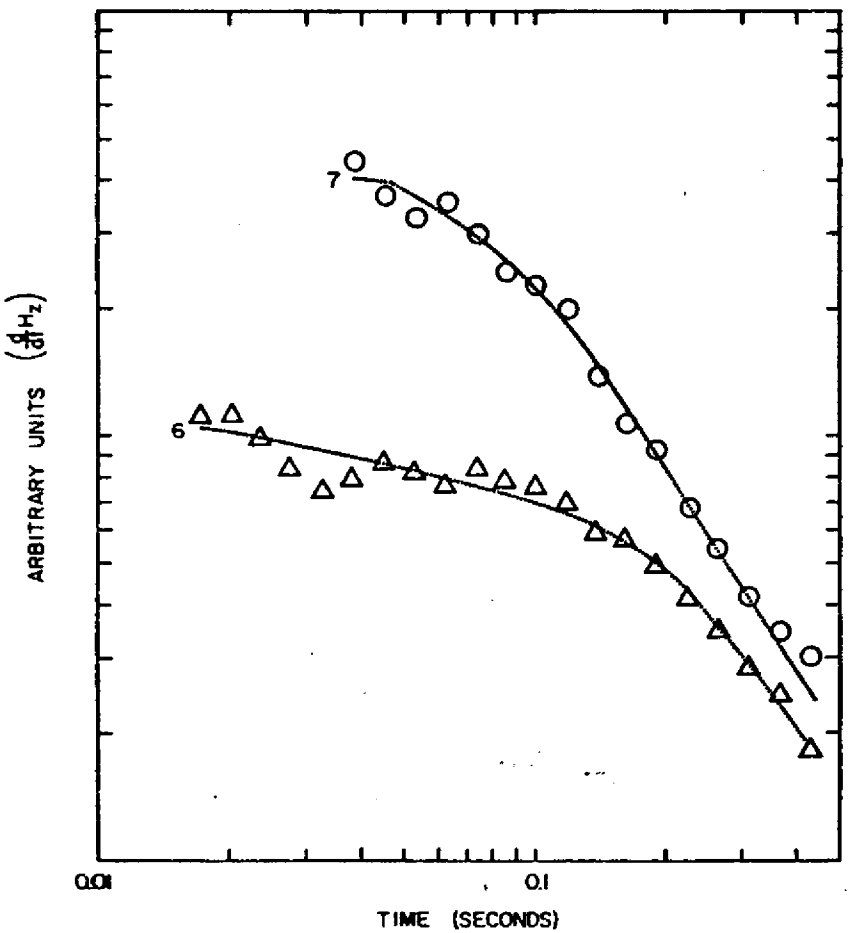

Puna TDEM sounding 6(1)

parameter correlation matrix

	σ_1	σ_2	σ_3	d_1	d_2
σ_2	.96				
σ_3	.83	.93			
d_1	-.46	.70	-.77		
d_2	-.97	-.99	-.89	.65	
fctr	.94	1.0	.94	-.73	-.99

final parameters

σ_1	.15	± big
σ_2	.33	± big
σ_3	2.6	± big
d_1	251.	± big
d_2	902.	± big
fctr	1.58	± big

Puna TDEM sounding 7(1)

parameter correlation matrix

	σ_1	σ_2	σ_3	d_1	d_2
σ_2	-.90				
σ_3	-.93	.99			
d_1	-.96	.92	.94		
d_2	-.80	-.97	-.94	-.81	
fctr	-.92	1.0	.99	.94	-.96

final parameters

σ_1	.0041	± big
σ_2	.20	± big
σ_3	1.41	± big
d_1	246.	± big
d_2	1007.	± big
fctr	1.506	± big

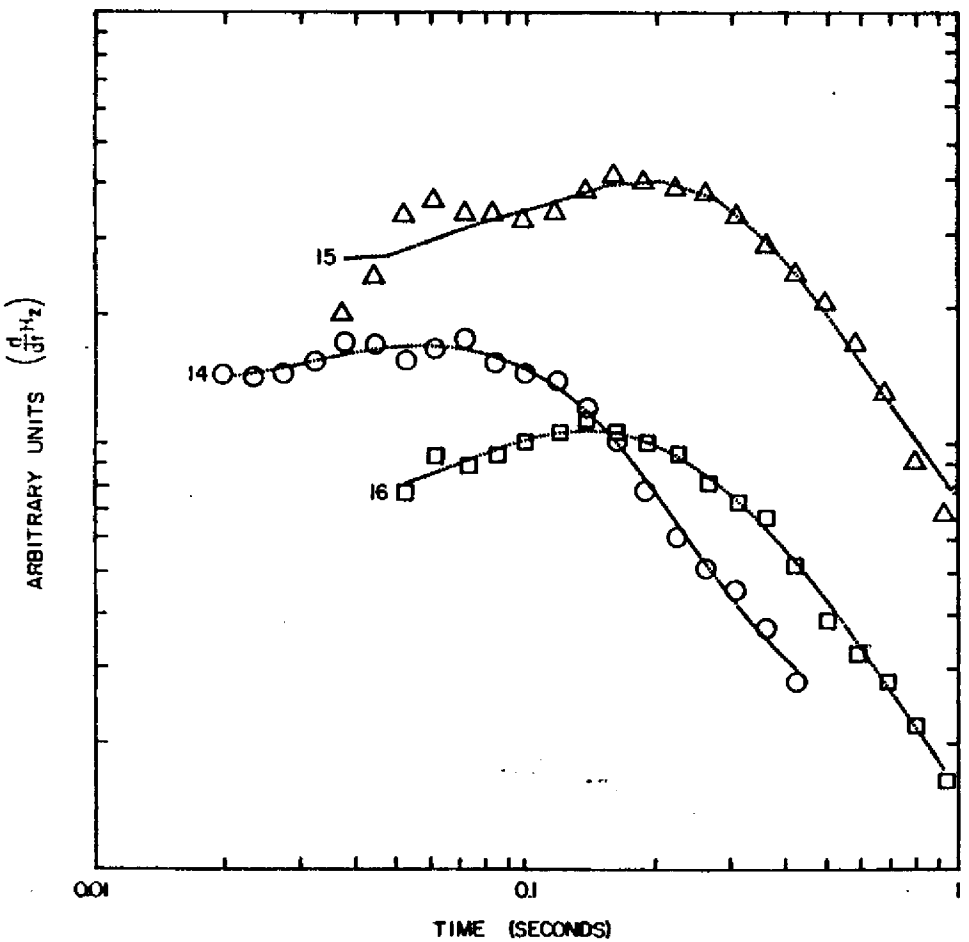

Puna TDEM sounding 14(1)

parameter correlation matrix

	σ_1	σ_2	σ_3	d_1	d_2
σ_2	-.97				
σ_3	-.96	.98			
d_1	-.95	.96	.99		
d_2	.84	-.89	-.94	-.97	
fctr	-.92	.96	.99	.99	-.98

final parameters

σ_1	1.8	± 58%
σ_2	.58	± 93%
σ_3	14.6	±382%
d_1	46.4	±266%
d_2	326.	± 78%
fctr	3.05	± big

Puna TDEM sounding 15(1)

parameter correlation matrix

	σ_1	σ_2	σ_3	d_1	d_2
σ_2	-.72				
σ_3	-.94	.91			
d_1	-.99	.78	.96		
d_2	-.77	.23	.55	.70	
fctr	-.81	.98	.96	.86	.30

final parameters

σ_1	2.9	±421%
σ_2	.254	± 65%
σ_3	.89	±907%
d_1	18.7	±567%
d_2	1091.	± 70%
fctr	1.29	±105%

Puna TDEM sounding 16(1)

parameter correlation matrix

	σ_1	σ_2	σ_3	d_1	d_2
σ_2	.81				
σ_3	-.82	-.43			
d_1	-.96	-.94	.70		
d_2	.39	.84	.11	-.61	
fctr	-.58	-.19	.92	.46	.29

final parameters

σ_1	2.35	± 73%
σ_2	.163	±163%
σ_3	.429	± 71%
d_1	30.3	±171%
d_2	535.	± 71%
fctr	1.103	± 10%

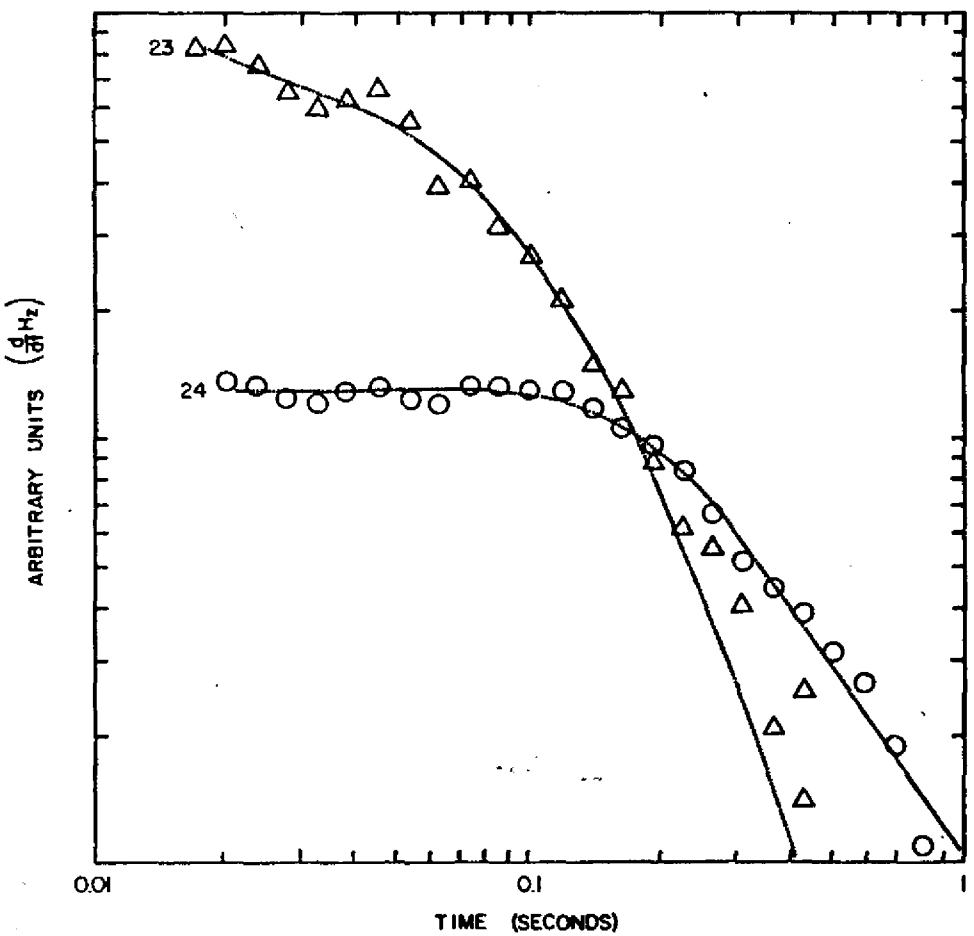

Puna TDEM sounding 23(3)

parameter correlation matrix

	σ_1	σ_2	σ_3	d_1	d_2
σ_2	.39				
σ_3	.56	.82			
d_1	.26	.95	.62		
d_2	-.52	-.97	-.93	-.86	
fctr	-.14	.62	.70	.47	-.63

final parameters

σ_1	.15	± 34%
σ_2	.54	±101%
σ_3	.015	± big
d_1	243.	± 41%
d_2	258.	±230%
fctr	1.127	± 12%

Puna TDEM sounding 24(3)

parameter correlation matrix

	σ_1	σ_2	d_1
σ_2	.97		
d_1	-.89	-.77	
fctr	1.0	.97	-.90

final parameters

σ_1	.38	± 18%
σ_2	1.34	±114%
d_1	911.	± 19%
fctr	1.206	± 19%

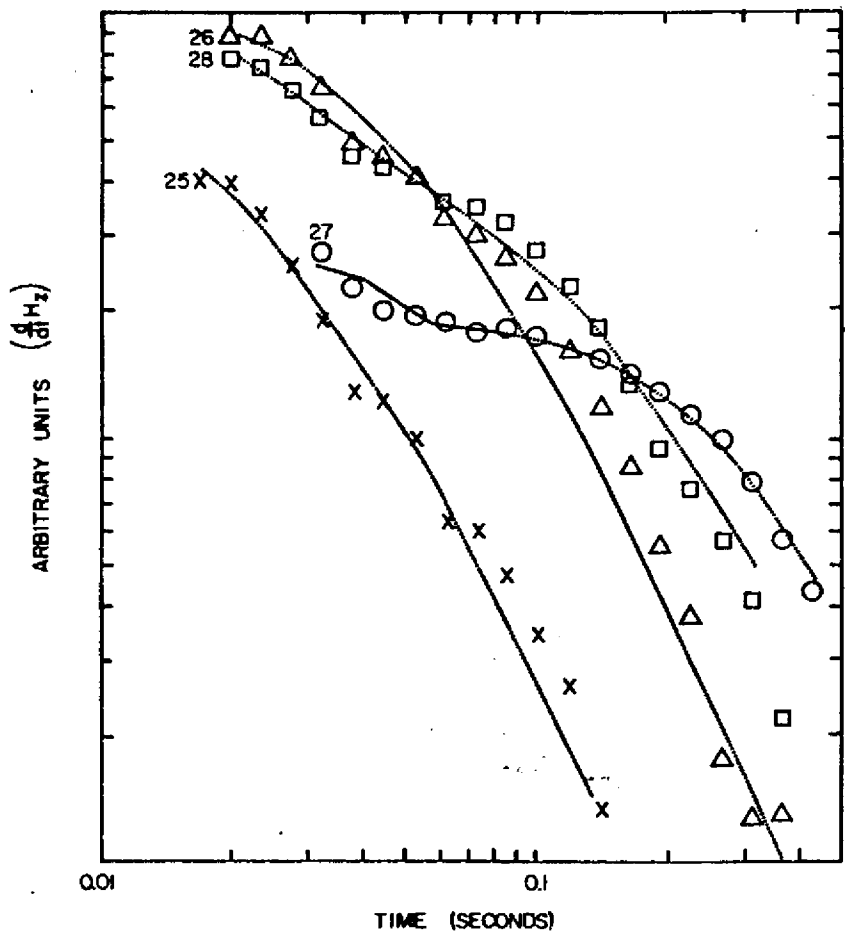

Puna TDEM sounding 25(4)

parameter correlation matrix

	σ_1
fctr	-.17

final parameters

σ_1	.055 ± 5%
fctr	1.296 ± 2%

Puna TDEM sounding 26(4)

parameter correlation matrix

	σ_1	σ_2	d_1
σ_2	.71		
d_1	-.99	-.78	
fctr	.05	.69	-.17

final parameters

σ_1	.15 ± big
σ_2	.076 ± 14%
d_1	21.5 ± big
fctr	1.035 ± 1%

Puna TDEM sounding 27(4)

parameter correlation matrix

	σ_1	σ_2	d_1	d_2
σ_2	-.89			
d_1	-.90	.98		
d_2	.89	-1.0	-.98	
fctr	-.87	.96	.95	-.94

final parameters

σ_1	.02<5	± 21%
σ_2	.68	± 81%
σ_3	1.e-5	fixed
d_1	794.	± 24%
d_2	272.	± 78%
fctr	1.371	± 14%

Puna TDEM sounding 28(4)

parameter correlation matrix

	σ_1	σ_2	d_1	d_2
σ_2	.86			
d_1	-.30	-.69		
d_2	-.83	-.99	.75	
fctr	.69	.96	-.86	-.97

final parameters

σ_1	.061	± 60%
σ_2	.265	± 71%
σ_3	2.	fixed
d_1	461.	± 11%
d_2	872.	± 98%
fctr	1.557	± 29%

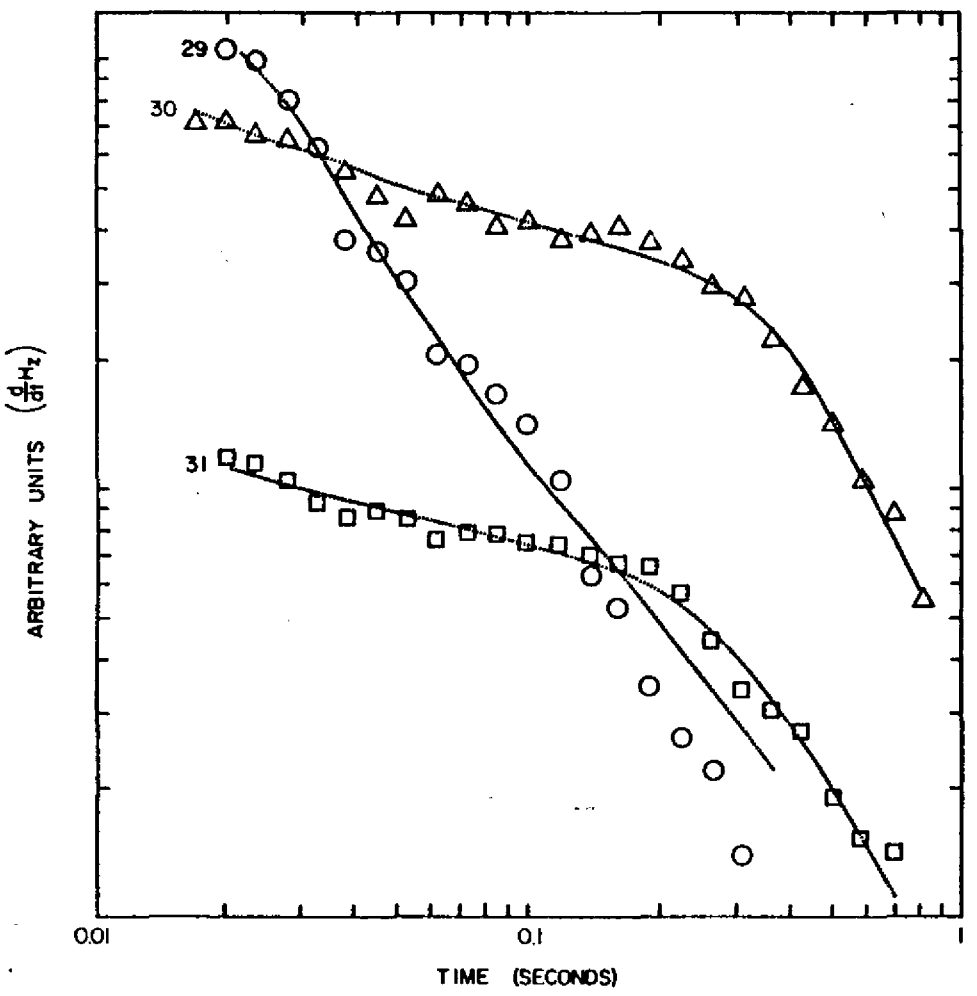

Puna TDEM sounding 29(4)

parameter correlation matrix

	σ_1	σ_2	d_1
σ_2	.96		
d_1	-.74	-.72	
fctr	.84	.87	-.94

final parameters

σ_1	.025	± 17%
σ_2	.19	± 76%
d_1	1225.	± 11%
fctr	1.535	± 10%

Puna TDEM sounding 30(4)

parameter correlation matrix

	σ_1	σ_2	σ_3	d_1	d_2
σ_2	.94				
σ_3	-.57	-.50			
d_1	-.89	-.98	.50		
d_2	-.96	-.99	.61	.97	
fctr	.94	1.0	-.51	-.99	-.99

final parameters

σ_1	.082	± 76%
σ_2	.33	± 85%
σ_3	21.5	±300%
d_1	306.	± 33%
d_2	1302.	± 94%
fctr	1.88	± 72%

Puna TDEM sounding 31(4)

parameter correlation matrix

	σ_1	σ_2	σ_3	d_1	d_2
σ_2	.94				
σ_3	.57	.72			
d_1	-.06	-.37	-.53		
d_2	-.95	-.99	-.63	.33	
fctr	.92	1.0	.73	-.43	-.99

final parameters

σ_1	.12	± 86%
σ_2	.29	± 85%
σ_3	3.1	±148%
d_1	293.	± 30%
d_2	1196.	±113%
fctr	1.474	± 67%